Basha Shaik, Nagoor ; Inayat, Muddasser; Benjapolakul, Watit ; Bakthavatchalam, Balaji ; D Barewar, Surendra ; Asdornwised, Widhyakorn ; Chaitusaney, Surachai

Artificial Neural Network Modeling and Optimiztion of Thermophysical Behavior of 1 MXene Ionanofluids for Hybrid Solar Photovoltaic and Thermal Systems

Published in:
Thermal Science and Engineering Progress

DOI:
10.1016/j.tsep.2022.101391

Published: 01/08/2022

Document Version
Peer-reviewed accepted author manuscript, also known as Final accepted manuscript or Post-print

Please cite the original version:
Basha Shaik, N., Inayat, M., Benjapolakul, W., Bakthavatchalam, B., D Barewar, S., Asdornwised, W., & Chaitusaney, S. (2022). Artificial Neural Network Modeling and Optimiztion of Thermophysical Behavior of 1 MXene Ionanofluids for Hybrid Solar Photovoltaic and Thermal Systems. *Thermal Science and Engineering Progress*, *33*, Article 101391. https://doi.org/10.1016/j.tsep.2022.101391

Artificial Neural Network Modeling and Optimiztion of Thermophysical Behavior of MXene Ionanofluids for Hybrid Solar Photovoltaic and Thermal Systems

Nagoor Basha Shaik[1], Muddasser Inayat[2], Watit Benjapolakul[1, *], Balaji Bakthavatchalam[3], Surendra D Barewar[4], Widhyakorn Asdornwised[1] and Surachai Chaitusaney[1]

[1]Artificial Intelligence, Machine Learning, and Smart Grid Technology Research Unit, Department of Electrical Engineering, Faculty of Engineering, Chulalongkorn University, Bangkok 10330, Thailand.

[2]Research Group of Energy Conversion, Department of Mechanical Engineering, School of Engineering, Aalto University, 02150 Espoo, Finland.

[3]Department of Mechanical Engineering, Amrita School of Engineering, Amrita Vishwa Vidyapeettham, Chennai, Tamilnadu, India.

[4]School of Mechanical and Civil Engineering, M.I.T. Academy of Engineering, Alandi, Pune-412105, India.

[*]Corresponding email: watit.b@chula.ac.th

Abstract

Newly developed MXene materials are excellent contender for improving thermal systems' high energy and power density. MXene Ionanofluids are novel materials; their optimum thermophysical behavior at various synthesis conditions has not been addressed yet. The aim of this study is to investigate the effect of synthesis conditions (temperature 303-343 K and nanofluids concentration 0.1-0.4 wt.%) on the thermophysical properties (thermal conductivity, specific heat capacity, thermal stability, and viscosity) of MXene Ionanofluids. Levenberg Marquardt based Artificial Neural Network (ANN) model and Response Surface Methodology (RSM) based optimization techniques have been adopted for systematic parametric analysis of MXene Ionanofluids thermophysical properties using experimental data. ANN and RSM have predicted the thermophysical behavior of MXene ionanofluids at optimized conditions. The experimental data were used to train, test, and validate the ANN model. The neural network could correctly predict the outcomes for the four properties based on the numerical performance with R^2 values close to 1, and a prediction error is 2%. The performance of the proposed LM-based back-propagation algorithm demonstrates that the error involved has been minimal and acceptable. RSM has developed correction among input parameters and thermophysical properties of MXene Ionanofluids. The comparison between experimental results and the proposed correlations revealed excellent practical compatibility.

Optimized thermophysical properties of MXene Ionanofluids thermal conductivity of 0.776 W/m.K, specific heat capacity of 2.5 J/g.K, thermal stability of 0.33931 wt. loss %, and viscosity of 11.696 mPa.s were obtained at a temperature of 343 K and nanofluids concentration of 0.3 wt.%. MXene Ionanofluids with optimal thermophysical properties could be used for the greatest performance of hybrid solar photovoltaic and thermal system applications.

Keywords: MXene Ionanofluids, Artificial Neural Networks, Response Surface Methodology, Solar energy, Thermophysical properties,

Highlights:

1. Thermophysical properties of MXene Ionanofluids are presented for PV/T system.
2. LMBPNN approach was used to predict the thermophysical behavior of MXene Ionanofluids.
3. LMBPNN model performance in predicting the thermophysical property behavior.
4. Optimization and Parametric analysis of thermophysical properties was performed using RSM.

1 Introduction

MXenes are two-dimensional (2D) materials synthesized by etching the 'A' element from the MAX phases of metal carbides and carbo-nitrides. Since its discovery in 2011, MXene proved to be a great candidate for enhancing thermal systems' high energy and power density. Its distinguishing characteristics, including exceptional biocompatibility, high conductivity, and eco-friendliness, drive its widespread appeal. Usually, nanoparticles (graphene, aluminum, zinc, etc.) are combined with base fluids (water, glycols, and oils) to produce an enhanced heat transfer fluid known as "nanofluid." Nanofluids can be made more stable using ionic liquids. Ionic liquids' anions and cations provide an electrostatic layer around nanoparticles that keeps them from accumulating. The long alkyl chains in cations of ionic liquids help ensure nanoparticle stability in a suitable solvent [1-3]. Therefore, nanofluids are suspended in ionic liquids (Ionanofluids) to obtain desired properties and functions such as excellent thermal properties, high light absorbance, and conductivity. MXene nanoparticles are synthesized and incorporated with ionic liquids to develop an innovative fluid called "MXene Ionanofluids." The primary goal of incorporating MXene nanoparticles with heat transfer fluids (ionic liquids and base fluids) is to improve their thermophysical characteristics. Density, viscosity, specific heat capacity, and thermal conductivity are some of these characteristics to consider. For instance, Agresti et al. enhanced the efficiency of perovskite solar cells using MXene (Ti_3C_2Tx), where the authors reported a maximum power conversion improvement of 26% [4]. MXene based Ionanofluids have the potential to be employed as heat transfer fluids in photovoltaic thermal systems (PV/T) due to their fascinating thermophysical and optical properties [5]. Abdelrazik et al. optimized the performance of a hybrid PV/T system using MXene/water nanofluids that attributed to high light absorption compared to conventional working fluids [6]. Aslfattahi et al.[7] improved the efficiency of a solar collector using MXene/Soybean oil, resulting in a thermal efficiency of 82.66% and a daily yield of 9.07 kWh. Furthermore, Samylingam et al. [8] enhanced the thermal and energy performance of hybrid PV/T systems utilizing MXene/Olein palm oil with a maximum improvement of 16% thermal efficiency and 9% heat transfer. These studies proved that MXene has a significant influence on PV/T systems. Using experimental techniques and precise laboratory instruments is reliable and accurate results. Hakan et al. used energy and exergy analysis methods based on the first and second principles of thermodynamics to examine the performance of porous baffles with varying thicknesses installed in solar air heaters (SAHs). They evaluated five different types of SAHs and compared their efficiency. Their findings revealed that SAHs with a thickness of 6 mm and an air mass flow rate of 0.025 kg/s produce the maximum collector efficiency and air temperature rise [9]. Unfortunately, the above investigations (experimental approaches) are time-consuming and expensive, but it is necessary to understand the thermophysical properties of working fluids (nanofluids or Ionanofluids) for different parameters (varying concentrations, particle sizes etc.).

Soft computing technologies such as artificial neural networks (ANN), fuzzy logic, and genetic algorithms have gained popularity to minimize these costs in the last decade. Artificial Intelligence (AI) enabled neural networks may significantly reduce the amount of time and money needed to tackle complicated problems across a wide range of fields. Figure 1 depicts the general framework of an evolutionary system for designing and training neural networks [10]. In recent years, ANN-based models have been increasingly popular for analyzing the non-linear behavior of Ionanofluid's thermophysical properties in thermal systems. The use of ANN networks to predict the thermophysical properties of MXene Ionanfluids for PV/T systems is not widely discussed. Using a genetic algorithm (GA) and mind evolutionary algorithm (MEA), Wang et al. [11] developed a model to estimate the thermal conductivity of hybrid nanofluids for waste heat systems. Fatih et al. explored the effects of a magnetic dipole source on natural ferrofluid convection in a triangular cavity. They solved the governing equations of a linked multi-physics system using the finite element method (FEM), and calculations were done for various parameter ranges [12].

Yang et al. [13] applied an ANN model using Levenberg Marquardt for predicting the thermal conductivity of mono, binary and ternary nanofluids. For the selected 102 samples, the maximum absolute error was less than 0.018. Based on the experimental data, Ji et al. [14] proposed two ANN models, and the relative error is considered for optimizing the size of the networks. The authors reported a maximum relative error of 1.4% and 3.5% for thermal conductivity and viscosity of TiO_2-Ag hybrid nanofluids, which saved a lot of time and money. With perceptron feed-forward ANN (FFNN), Tian et al. [15] assessed the thermal properties of graphene based nanofluids with varying temperature and volume fractions. The results indicated that ANN's mean square error (MSE) and thermal conductivity correlation coefficient are on the order of $1.67e^{-6}$ and 0.99, respectively. An optimal nanoparticle mixing ratio is employed by Malika et al. [16] to forecast the thermal conductivity ratio of Fe_2O_3-SiC/water nanofluid using ANN (multilinear perceptron approach) and RSM (Response Surface Methodology). Based on their results, the ANN model predicted the Fe_2O_3-SiC/water nanofluid's thermal conductivity ratio more precisely than the RSM model. Abidi et al. [17] investigated the thermal performance of SiO2/EG-water nanofluid in a vacuum tube solar collector with an ANN model. Temperature prediction using the ANN model resulted in a maximum error of 7%, and the R^2 value was greater than 0.88 for the instantaneous efficiency of the collector. Bakthavatchalam et al. [18] performed ANN (LM technique) based modeling using experimental results for thermophysical properties measurement of MWCNT based nanofluids. With five input layers and the 'n' number of neurons, the R^2 value was almost close to one. Geetha et al. investigated different ANN models with three popular algorithms that were trained using meteorological data collected over a year from six different locations in India's hot areas for estimating hourly average global radiation for the purpose of designing or evaluating PV installations in areas without meteorological data collection facilities [19] In another study, Hakan and his team used FEM to calculate the shape impacts of TEG-mounted vented cavities on the performance characteristics of alumina-water nanofluid convection. They created an ANN model that produced correct power outputs for all cavity shapes [20]. The same group developed a hybrid approach for TEG power production in bifurcating channels using a hybrid nanofluid by combining ANN and CFD. The hybrid ANN + CFD technique reduced the computational time from 6 hours to 3 minutes [21]. Naman et al. used experimental data to create two FFNN models that solely took into account two properties of MXene materials: thermal conductivity and viscosity[22]. The same group suggested an ANN method to estimate the dynamic viscosity of MXene-palm oil nanofluid [23]. A similar study to predict thermal conductivity using ANN and the correlation between the parameters was carried out by Chitra et al. [24]. Based on the discussed literature, ANN techniques showed fewer errors when compared to the present correlations. Furthermore, the predicted ANN results of these works were in good agreement with the experimental results.

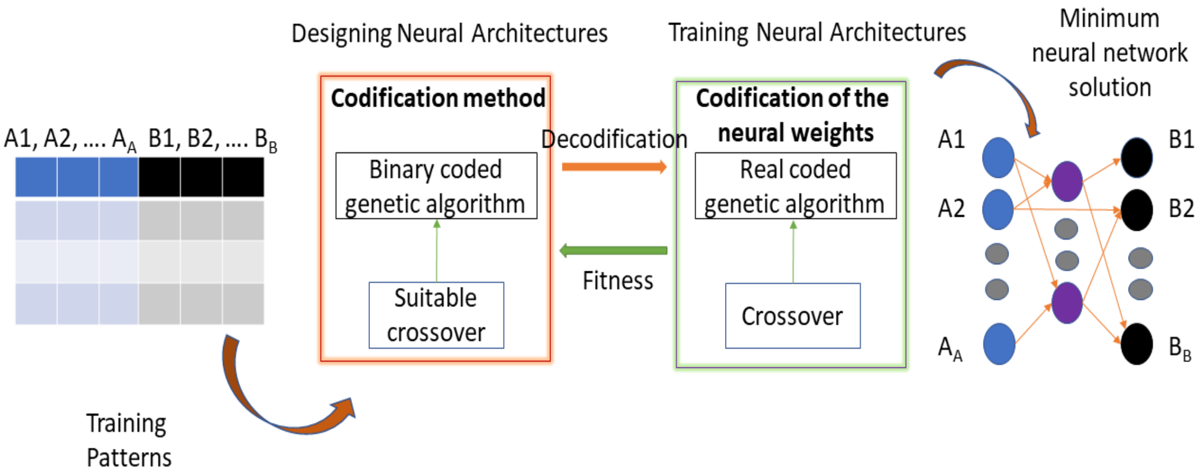

Figure 1: Typical structure of an evolutionary system to design and train ANN [10]

According to the authors' comprehensive knowledge, the literature did not investigate ANN modeling and parametric analysis of MXene Ionanofluid's thermophysical properties. Most studies used ANN to anticipate thermophysical properties, but no study attempted to develop ANN and perform parametric analysis at the same time for MXene materials ionanofluids. Significantly few methodologies for analyzing the properties of these MXene nanoparticles have been established. Still, the thermophysical properties behavior and its parametric analysis of ionanofluids of Mxne materials have not been addressed. Therefore, a new framework is provided based on ANN and RSM approaches for forecasting the thermophysical property behavior and parametric analysis of MXene ionanofluids. Furthermore, previous studies only evaluated one or two properties (i.e. thermal viscosity or thermal conductivity or both or another property), whereas the current work investigates the thermophysical behavior of four MXene Ionanofluids properties (viz. viscosity, thermal stability, thermal conductivity, and specific heat capacity) for hybrid Solar PV/T System applications. In addition, parametric analysis of these four characteristics is performed in the current work using RSM.

The present study proposes modelling and optimaztion of MXene Ionanofluids thermophysical properties for PV/T systems using ANN. An optimized neural network was created using eight hidden neurons and two inputs (temperature and nanoparticle concentration) in the ANN structure. The best performing network was selected based on its high correlation coefficient and low mean square error (MSE). A simple correlation has been presented using temperature and nanoparticle concentration. The prediction of thermophysical properties of MXene Ionanofluids was made using ANN; RSM techniques were applied for the parametric analysis and compared with ANN results for the first time to MXene Ionanofluids by analyzing the effect of nanoparticle concentration and temperature. Finally, MSE and the coefficient of determination (R^2) are used to validate the model's performance.

2 Methodology

Figure 2 depicts the overall methodology. This section is structured so that the first phase addresses the data collected from the experimental results. The second phase includes the development of the ANN model, and the third phase includes the parametric analysis of the thermophysical properties of Ionanofluids.

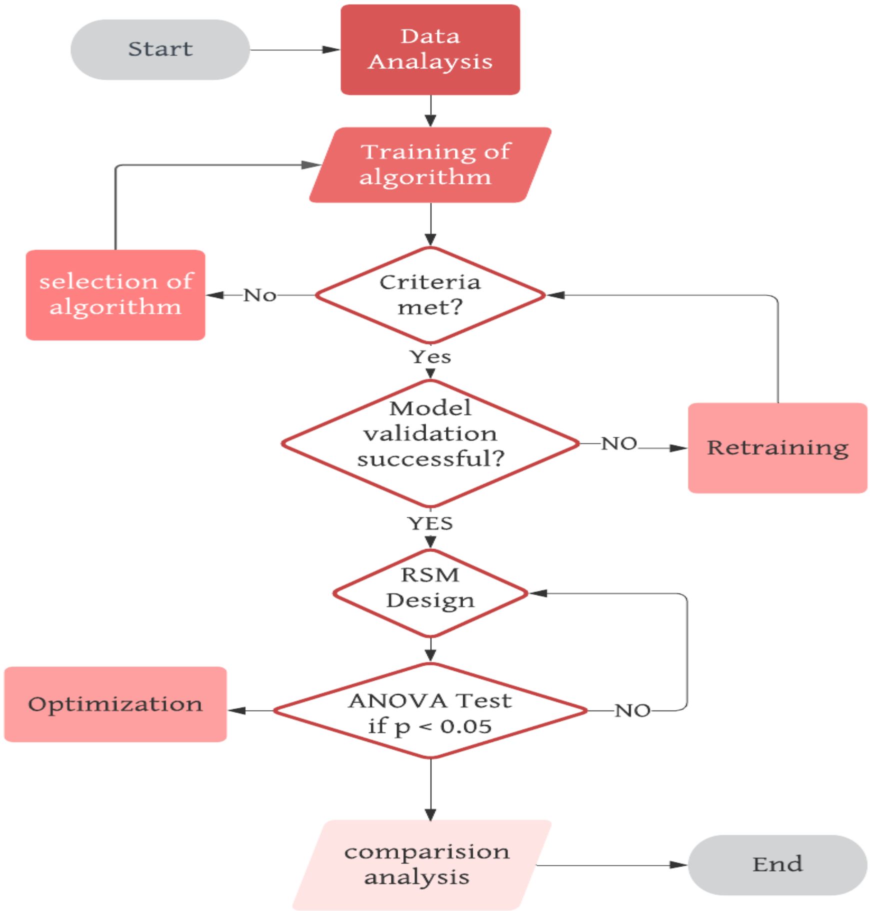

Figure 2: Flowchart of the proposed methodology

2.1 Data collection

Details on how to synthesize nanoparticles and prepare nanofluids can be found in [5]. The reported work includes a thorough characterization of the obtained MXene-Ionic nanofluid. This experimental study is then used to perform data regression using the LM based back-propagation algorithm. The analyzed data was then used to perform modeling of Ionnanofluid's thermophysical properties.

2.2 ANN model development

ANN is influenced by the human brain, which includes built-in neuron process units which can process input data and knowledge [25]. Input, hidden, and output layers are part of the multilayer perceptron neural network. The LM based back propagation neural network (BPNN) model is used in this work to predict the thermophysical properties of Ionnanofluid behavior. The input number is two, including temperature (K) and concentration (%), whereas the output number is one, includes thermophysical property (thermal stability/viscosity/conductivity/specific heat capacity). The neuron is the fundamental unit of the neural network. Each neuron weighs and adds input value, then sums to a bias parameter and passes the sum to a function known as the transition or activation function [26]. The transfer function calculates the outcome from the input of a neuron. The dataset is split into 3 different sets: train, validate, and test. 70% of the data is train data, the validate data is 15%, and the test data is 15% are considered. The weight and bias of each neuron are produced during the training phase. During the training of ANN, parameters are defined, and stop criteria are defined so that the network can be not overfitted. The selected algorithm used in the present work is Levenberg Marquardt for training the ANN with a maximum number of 1000 iterations.

The best design of the ANN was chosen according to the lowest difference between the experimental data values and expected (ANN output) data values. In order to determine the suitable configuration and assess the output and efficiency of the network, it is best to assume an average estimate after several iterations, given that splitting input data into three significant sets is random in every run of the program. Data has been chosen arbitrarily; several times, a network has been running for each structure. Following permutation, the most accurate and non-overfitting network architecture was selected. The best ANN architecture to estimate the thermophysical properties of nanofluid by presented requirements was with eight hidden neurons, comparing end performance with the optimized architecture is [2 8 1]. The ANN's model architecture receives variables of the temperature and concentration as inputs and then estimates thermal physical property using the activation function. The Levenberg-Marquardt Backpropagation (LMBP) algorithm is then performed to use the output function, dependent on an ANN estimation and thermal properties underlying realities. In addition to the weight values and bias variables, the back-propagation algorithm is used to calculate the Jacobian matrix. The ANN then calculates the output with adjusted weights and biases [27]. The LM based ANN model is well trained based on the above iterative processes. In the present work, the thermophysical properties are estimated by choice of a multilayer neural network. A single input, hidden, and output layer creates a single ANN. The ANN is built with a single hidden layer to manage the most complex functions. The multilayer ANN structure with weight links appears in Figure 3. The core feature of an ANN is the neuron. An LM model is designed to mimic a biological neuron's actions and functions. The neuron is biased and is added to the weighted inputs of the net input n, represented in equation (1) [28].

$$i_n = \sum_{j=1}^{m} w_j i_j + b \tag{1}$$

The transfer functions used in this work are 'tansig' and 'purelin' functions. The transfer functions can be seen in Figure 3. The equations can be defined by equations (2) and (3).

$$f_1 = {}^{2}/_{1 + e^{-x}} \tag{2}$$

$$f_2 = f(x) = x \tag{3}$$

The proposed LMBP neural network output is implemented by the following equation (4)

$$y = f_2\left(\sum_{k=1}^{s} w_l . f_1\left(\sum_{j=1}^{m} w_j i_j + b_1\right) + b_2\right) \tag{4}$$

where y indicates the total network output. m is the input number, S is the hidden layer neuron number, and i_j is the indicator of i^{th} input. The hidden layer and output layer activation functions are f_1 and f_2, respectively. b_1 and b_2 reflect the neuron biases of the hidden layer and the output layer. w_j is the weight connecting the input and the hidden layer, and w_l is the weight connecting the hidden layer with the output layer.

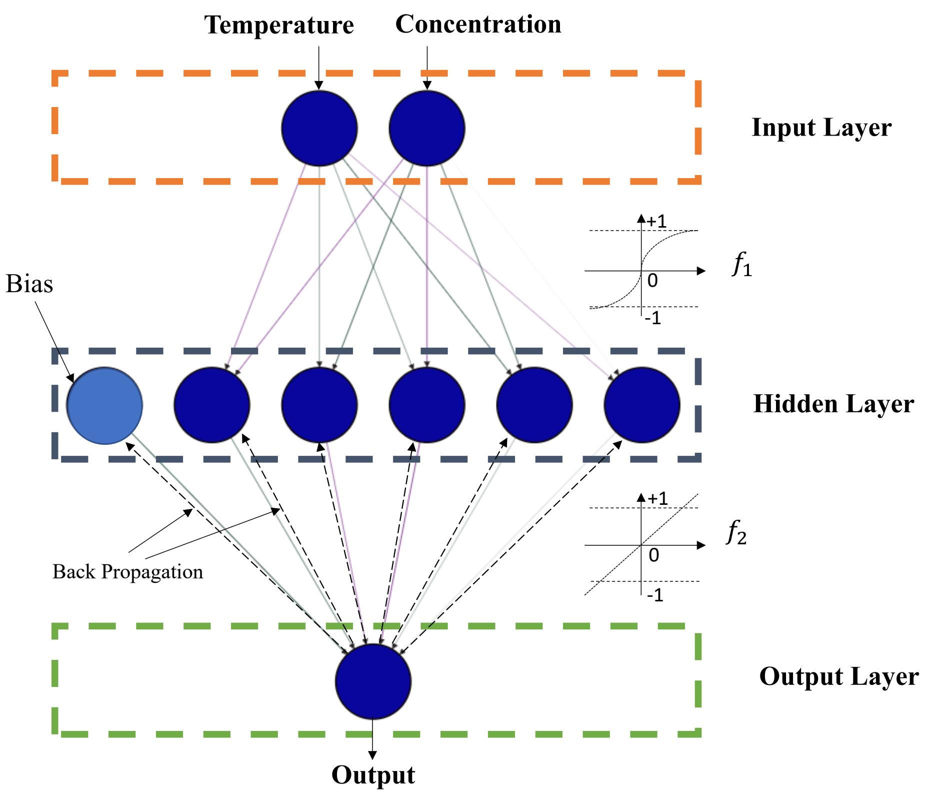

Figure 3: Neural network architecture

The complete learning LMBP can be summarised in three steps: 1) spread the input across the network, 2) spread the sensitivities backward from the last to the first layer through the network, 3) Use the estimated steepest descent rules to update the weights and biases. The BP algorithm is the steepest descent algorithm. LM is derived from the Newton method intended to minimize the number of functions in a square of non-linear functions. A process of iteration was used to find the exemplary network architecture. The best architecture was chosen based on the possible combinations of hidden neurons. The proposed LMBP neural network with 2 inputs, eight hidden neurons, transfer functions, and one output can be shown in Figure 4. The performance is checked using Mean squared Error (MSE), a loss function, and Coefficient of Determination (R^2). The MSE and R^2 values are calculated using equations (5) and (6).

$$MSE = \frac{1}{n}\sum_1^n (y - y_1)^2 \quad (5)$$

$$R^2 = 1 - \frac{\sum_1^n (y-y_1)^2}{\sum_1^n (y_{mean}-y_1)^2} \quad (6)$$

Where n is the number of data samples, y is actual, y_1 is predicted output

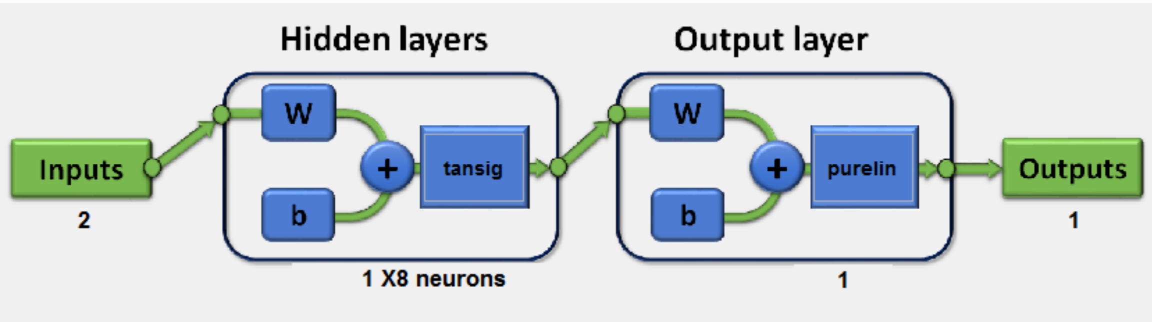

Figure 4: Proposed LMBP neural network

2.3 RSM design matrix development

Design of expert (DOE) v12 was used to develop the design array of response surface methodology (RSM) for experiments by using the Box Behnken Design (BBD) technique. RSM is a statistical tool used to determine a regression model for a quantitative data set. It is also optimized the process for various inputs and outputs at the same time. The three key steps in RSM are designed experiments, statistical analysis of a mathematical association of variables and responses, and response prediction [29, 30]. Two factors, three levels, RSM BBD technique, were used to evaluate the effect of formulating stable nanofluids concentrations [EMM][OSO_4]+DG+MXene (A) and temperature (B) on thermophysical characteristics of liquid such as viscosity, thermal conductivity, specific heat capacity, and thermal stability. The range of input variables was taken from previously published work [5], as shown in Table 1.

Table 1: Input variables range used for RSM experimental array using BBD.

Factor	Name	Units	Type	Minimum	Maximum	Coded Low	Coded High	Mean	Std. Dev.
A	[EMM][OSO_4]+ DG+MXene	wt.%	Numeric	0.1000	0.4000	-1 ↔ 0.20	+1 ↔ 0.40	0.2923	0.0862
B	Temperature	K	Numeric	303.00	343.00	-1 ↔ 308.00	+1 ↔ 338.00	323.00	11.90

DOE designed the array for thirteen experiments with five repeated experiments at central value. Their experimental response to viscosity, thermal conductivity, specific heat capacity, and thermal stability are given in Table 2.

Table 2. Experimental design array and their responses.

Std	Run	[EMM][OSO_4]+DG+MXene (wt.%)	Temperature (K)	Thermal conductivity (W/m.K)	Specific Heat Capacity (J/(g.K)	Thermal Stability wt. loss %	Viscosity (mPa.s)
1	1	0.2	308	0.521	2.27	0.84979	24.999
12	2	0.3	323	0.654	2.2	0.58801	18.725
9	3	0.3	323	0.641	2.18	0.60675	17.527
10	4	0.3	323	0.651	2.26	0.62545	16.645
5	5	0.1	323	0.485	2.5	0.56466	13.388
4	6	0.4	338	0.776	2.38	0.39111	17.523
8	7	0.3	343	0.773	2.43	0.33931	11.696
7	8	0.3	303	0.528	2.05	0.76366	31.112
3	9	0.2	338	0.687	2.55	0.47979	8.1166
2	10	0.4	308	0.621	1.91	0.74393	34.706
11	11	0.3	323	0.65	2.19	0.60535	18.255
6	12	0.4	323	0.711	2.23	0.59285	23.318
13	13	0.3	323	0.651	2.24	0.64453	16.125

3 Results and Discussion

This section is split into three subsections. The first subsection presents the findings of the data analysis for the Ionanofluid's thermal characteristics based on the experimental data collected. The second subsection covers the suggested LMBPNN modeling performance of thermophysical properties for MXene nanoparticles. RSM's parametric analysis of the Ionanofluid's thermal properties is discussed in the third sub-section.

3.1 Data analysis

3.1.1 *Thermal stability*

Thermal degradation caused by high heat scenarios in thermal systems is one of the primary causes of heat exchange and lubrication fluid failure. Thermal analysis was performed to determine the thermal degradation of the as-prepared samples to overcome this. This study used the experimental data collected during this analysis. Figure 5 depicts a visual representation of Ionanofluid's thermal stability property.

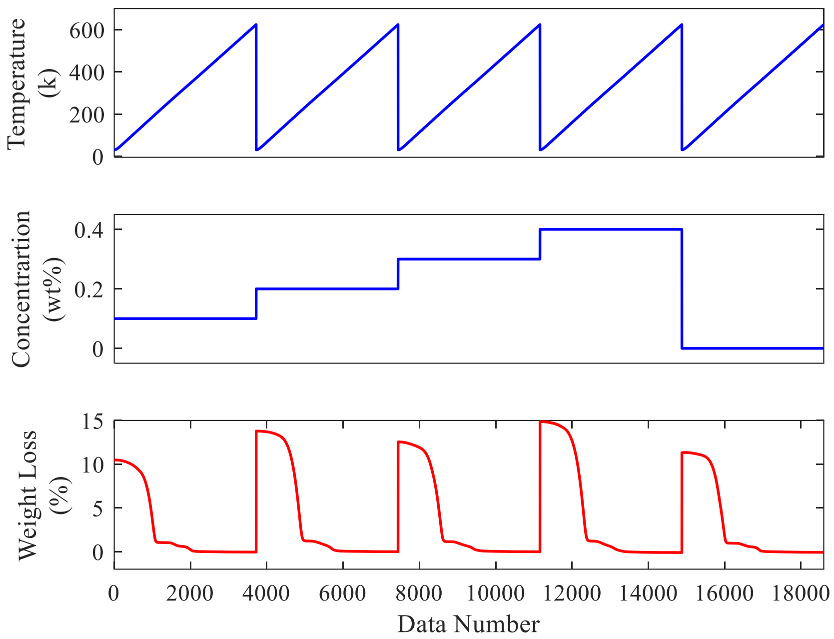

Figure 5: Data for thermal stability

3.1.2 Viscosity

The internal resistance can be measured with changes in temperature, pressure, and particle concentration using viscosity, a fundamental property of liquids. The viscosity of nanofluids is generally much higher than that of base fluids, and it rises even further when nanoparticles and ionic liquids are added. Figure 6 depicts the viscosity data visualization collected from the experimental study.

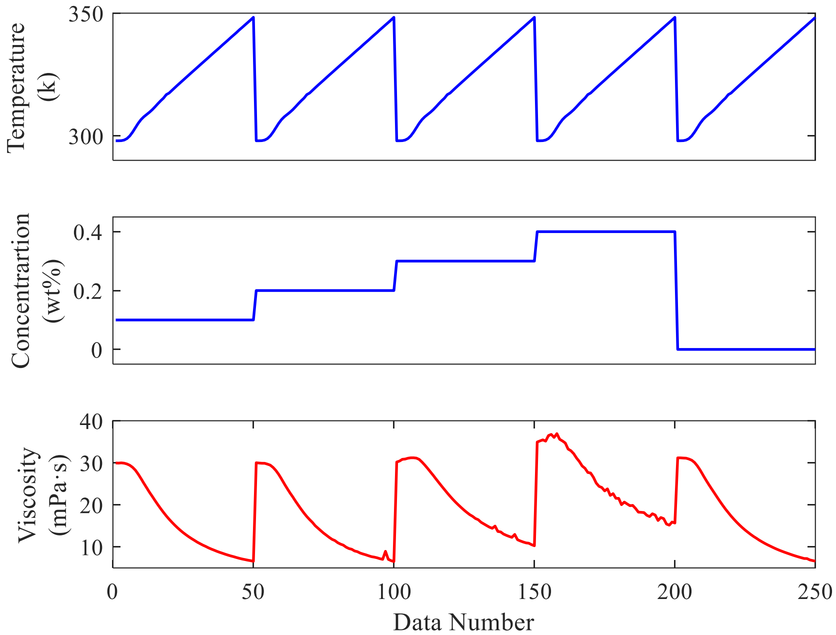

Figure 6: Data for Viscosity

3.1.3 Specific heat capacity

The experimental analysis was carried out, and the data was collected. Specific heat capacity is a fundamental property determining the amount of heat required to raise a substance's temperature. Figure 7 depicts Ionanofluid's specific heat capacity data.

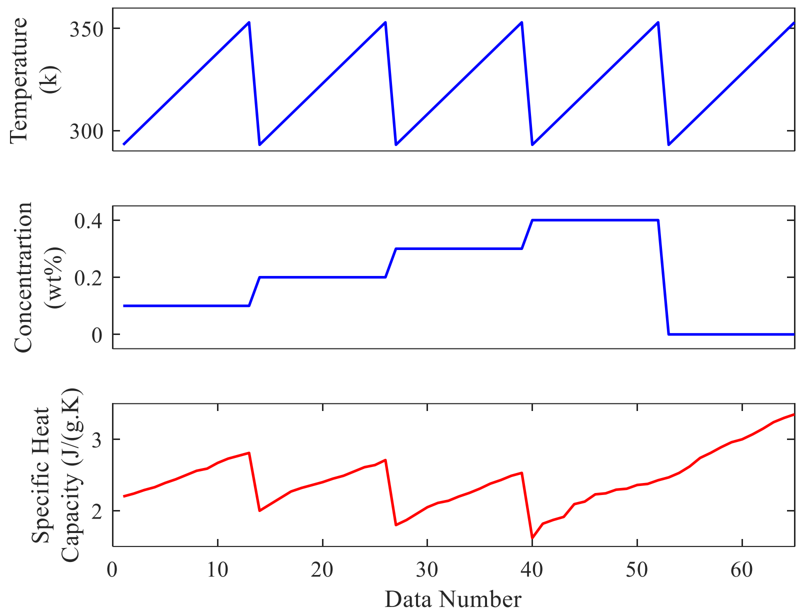

Figure 7: Data for Specific Heat Capacity

3.1.4 *Thermal conductivity*

Thermal conductivity is the measure of a medium's ability to conduct heat that is primarily determined by the material and temperature. Figure 8 depicts the data visualization of measured thermal conductivity values during the experiment.

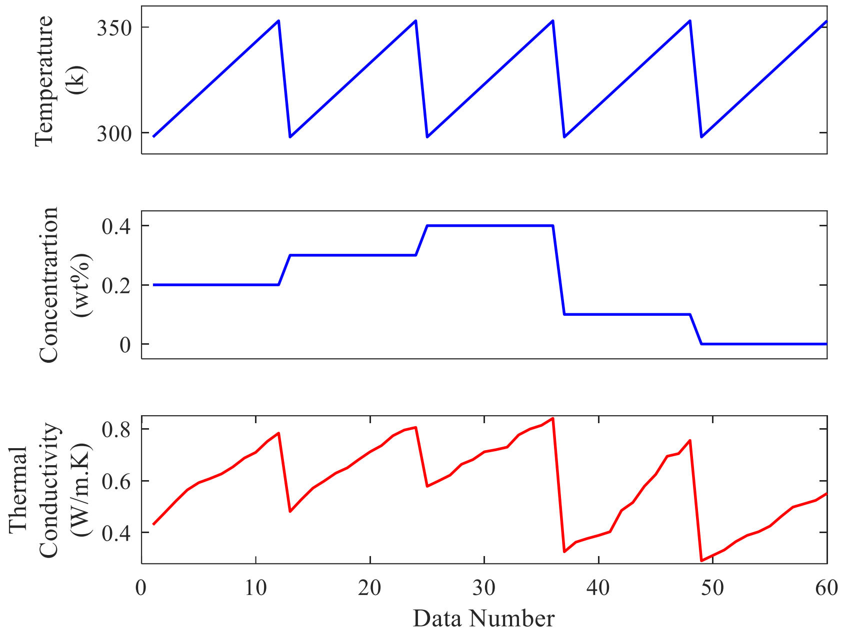

Figure 8: Data for Thermal Conductivity

3.2 LMBPNN Performance

This section examines the LMBPNN modeling of thermophysical properties for MXene nanoparticles. The numerical analysis for all these properties is performed first, followed by the predictions from the network during training, validation, and testing. Different BPA predictions for four properties are discussed separately.

The LMBPNN models that predict nanofluid's thermophysical properties from the training dataset, including temperature and concentration, are developed. Figure 9 displays the correspondence between experimental and predicted thermal viscosity values for training datasets during the training phase. As can be shown, most data are on or near the bisector, which shows a good association between experimental data and forecast results. This plot shows the proximity between the experimental evidence and the outcomes that the ANN predicts. In Figure 9, the maximal error (error differs from experimental value to forecast) is significantly less. Furthermore, it is shown that there is a strong agreement with the training findings. The developed algorithms performed well with overall R^2 values of 0.99895, 0.99963, 0.99872, and 0.99783 for the thermophysical properties of a) Thermal Stability, b) Viscosity, c) Specific heat capacity, and d) Thermal Conductivity, respectively. Based on the overall R^2 values, the current ANN models predicted slightly better thermophysical properties behavior than previous works [23, 24]. Notably, the current work examined four properties for analysis, whereas prior efforts only evaluated one or two properties.

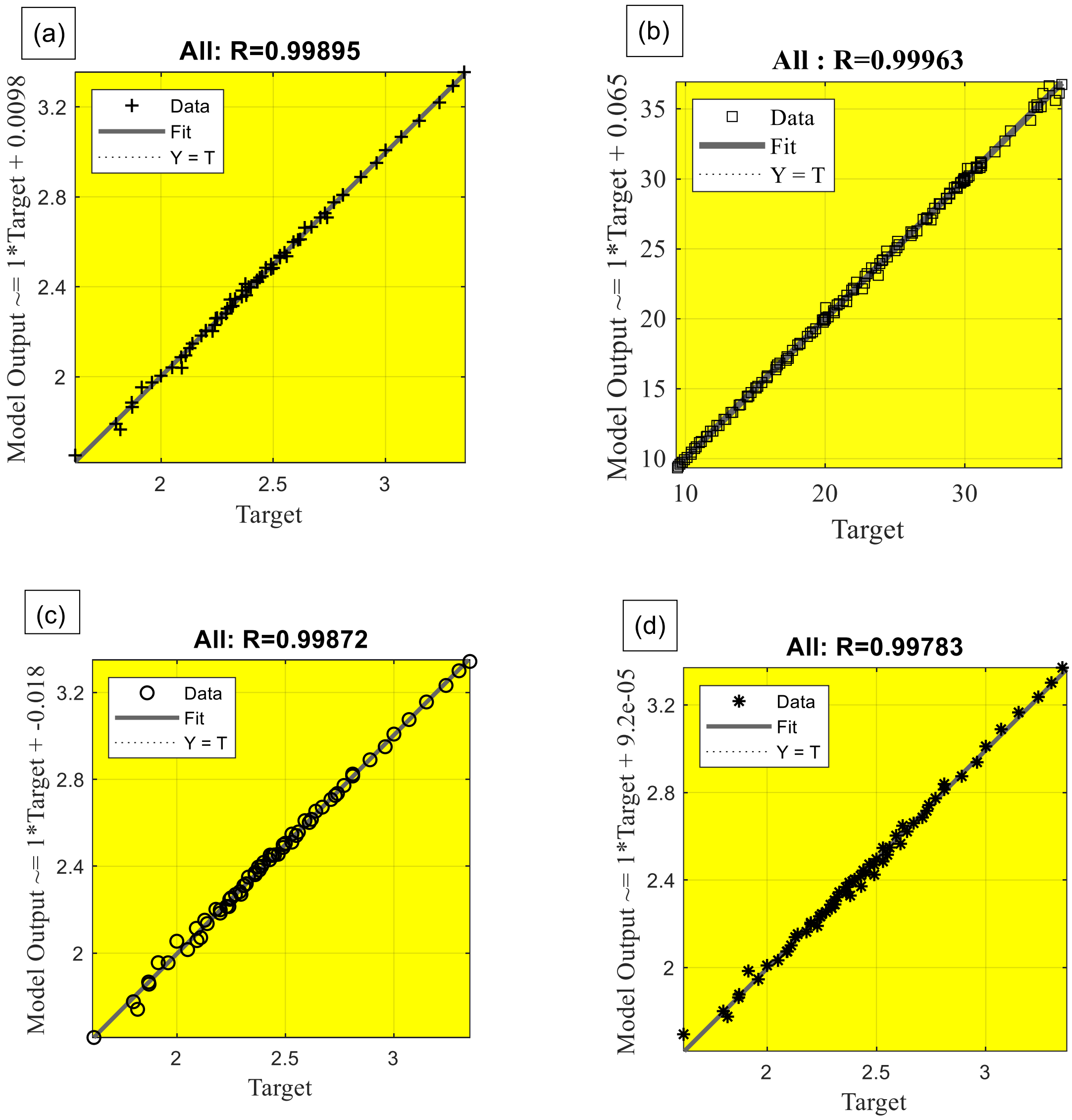

Figure 9: Linear Regression plots for all data used in training process a) Thermal Stability b) Viscosity c) Specific heat capacity d) Thermal Conductivity

Following the training of an LMBPNN neural network, Figure 10 is the histogram of errors between target values and expected values. Since these error values show if the forecast values vary from the target values, they should also be negative. Bins are the number of vertical bars on the chart. Y-axis reflects the number of samples in each dataset. Zero error line equivalent to zero error value on the error axis (i.e., X-axis). In this case, the zero-error point is below the 0.0015 central bin.

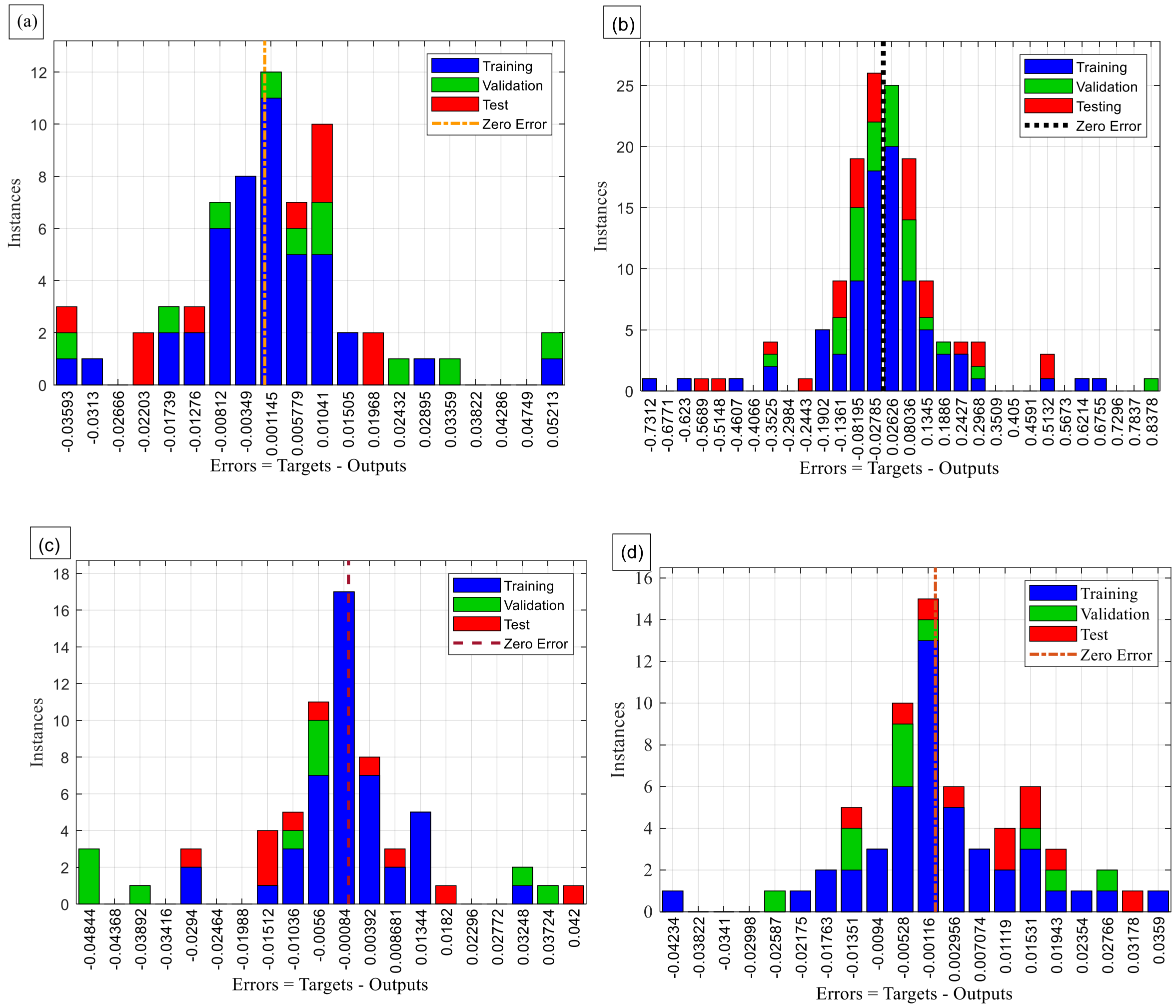

Figure 10: Error Histogram plot for training, validation, and testing data a) thermal stability b) viscosity c) specific heat capacity d) thermal conductivity

Numerical analysis is performed to determine the performance of the developed LMBPNN. For the LMBPNN accuracy evaluation, the MSE and R^2 are used. Equations (5) and (6) are used to estimate these parameters. The training performance of the LMBPNN models to predict thermophysical properties with temperature and concentration as inputs is worth noting. With 8 neurons in the hidden layer, the prediction, i.e., models' prediction, becomes more fit. Table 3 displays the R^2 and MSE values to show how close the experimental and network values are. If the R^2 value is close to one, it means the model predicts the output more accurately, indicating a good fit between the experimental and predicted values.

Table 3: Numerical Performance of LMBPNN

Property	Performance Indicator	Training	Validation	Testing
Thermal Stability	R^2	0.999450	0.996191	0.997029
	MSE	1.64563e-4	1.1745e-3	1.56639e-3
Viscosity	R^2	0.99365	0.99857	0.999734
	MSE	1.5415e-4	3.09301e-4	9.98857e-1
Specific heat capacity	R^2	0.99643	0.997372	0.05628
	MSE	1.09954e-4	1.67250e-4	1.25480e-4
Thermal Conductivity	R^2	0.999356	0.997057	0.997256
	MSE	1.77412e-4	2.48593e-4	2.21032e-4

Figure 11 shows the plot of the predicted performance of the neural network model for the given experimental data of thermal stability. The curve matches experimental findings well. In contrast between actual and expected values, ANN errors are noticed to be small and are confirmed by an MSE value in the thermal stability estimations. The suggested LMBPNN should be observed to estimate thermal stability correctly. The use of various neurons in the hidden layer is the reason for reaching an optimum network.

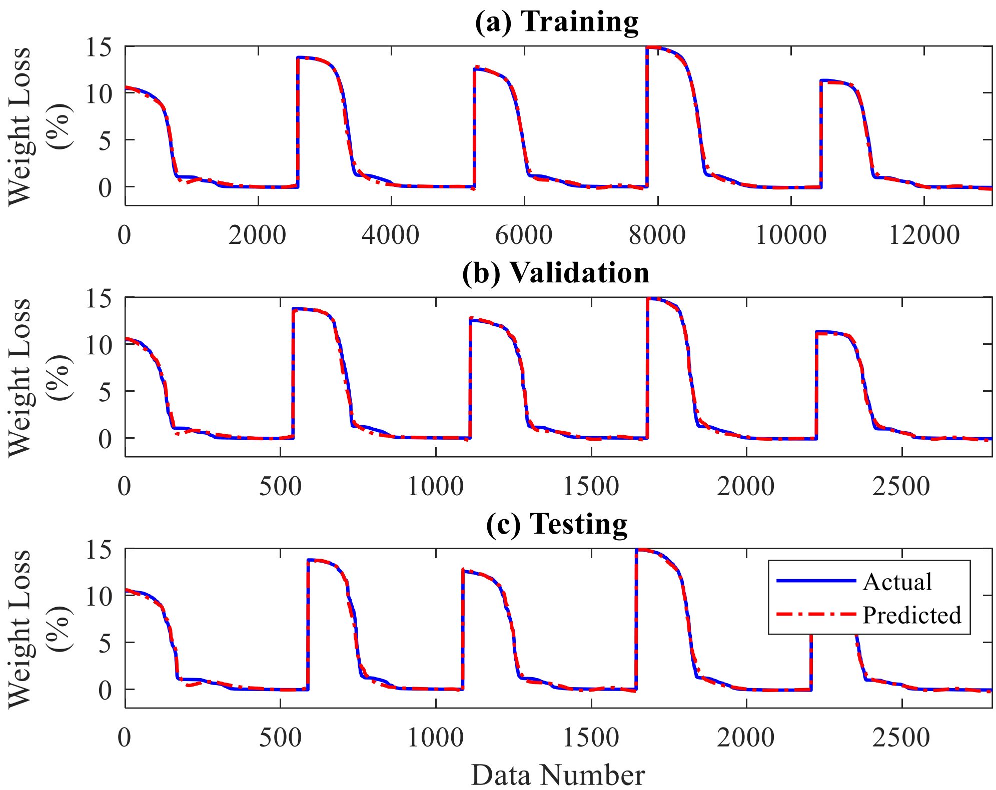

Figure 11: Training performance for thermal stability of proposed ANN

Figure 12 depicts the effect of the thermal viscosity estimate on the training, validation, and testing data sets. The x-axis shows data samples from the data collection, and the y-axis shows the effects of thermal viscosity estimation. As shown in Figure 12, the LMBPNN model produces high-precision outcomes, and the validation precision demonstrates that the approach produced is feasible and reliable.

The prediction of specific heat capacity using the LMBP algorithm is shown in Figure 13. The predictions are consistent with the results provided by LMBPNN. The model provides a good agreement and fits between the experimental and network outputs.

The results of the LMBPNN modeling performance for thermal conductivity are shown in Figure 14. Predicted results are found to be very close to experimental results. The model's data distribution for training, testing, and validation show fewer deviations, indicating a good model fitness in output prediction.

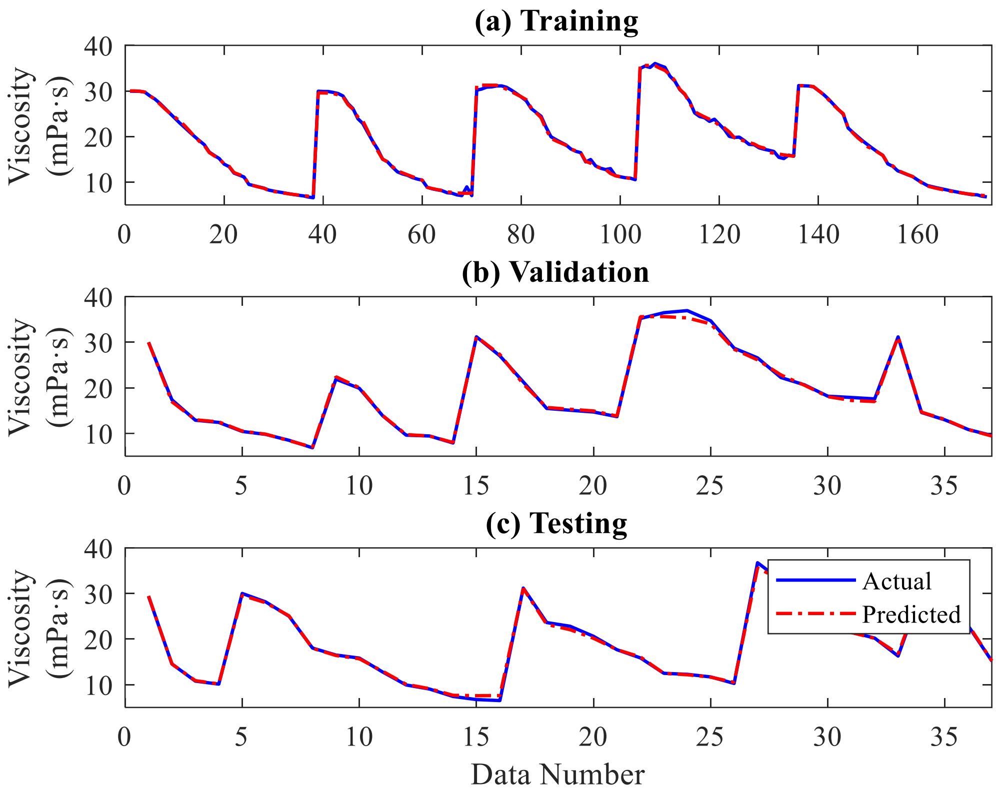

Figure 12: Training performance for viscosity of proposed ANN

Figure 13: Training performance for Specific Heat capacity of proposed ANN

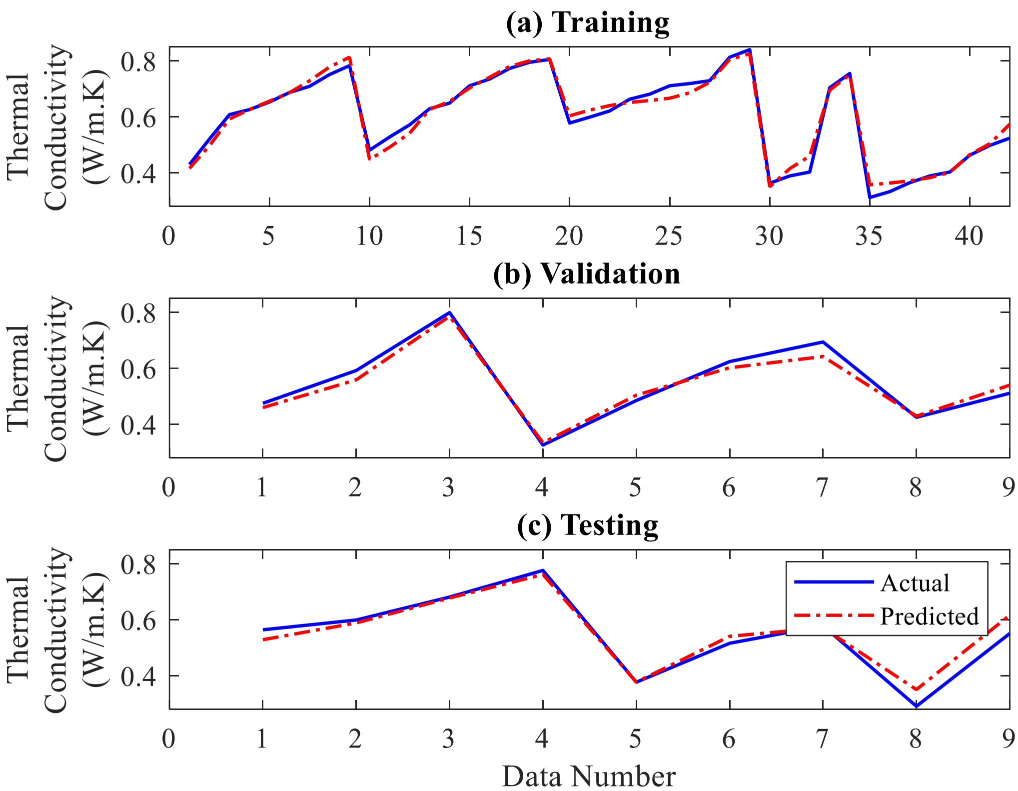

Figure 14: Training performance for thermal conductivity of proposed ANN

3.3 RSM statistical analysis

RSM evaluated statistically and graphically the thermophysical parameters of liquids such as viscosity, thermal conductivity, specific heat capacity, and thermal stability data. ANOVA analysis showed the significance of the variables and model terms, as shown in Table 4. The thermal conductivity, specific heat capacity, and thermal stability are modeled using ANOVA regression analysis. Three statistical tests, such as the model's significance and terms, lack of fit, and regression test, confirmed the model. The significance of the model and its terms values were described by a higher F-value and a lower P-value (value of probability). Model terms with a P-value of 0.05 (confidence level of 95%) are significant and closer to the actual experimental results. The differences between the measured and predicted value are referred to as lack of fit, indicating random or systematic data error [31]. The regression test R^2 evaluates the predicted model's overall accuracy and fitness for experimental results, with a range of 0 to 1.0.

A value of 1.0 indicates that the data is close to the actual value and significantly impacts the response. The Adj-R^2 denotes the variation in data that model fitted the data. The value of Pred-R^2 denotes the fitness and quality of model-predicted response data. The difference between Adj-R^2 and Pred-R^2 values indicates the model's quality, which should be less than 0.20 [32]. The non-significate model terms account for the more significant gap between Adj-R^2 and Pred-R^2. The development of 3D graphs and the interaction of operational factors and their effect on the response is a key component of RSM. Furthermore, the 3D response surface aids in obtaining intermediate points that could not be obtained by experimentation [33].

Table 4: Analysis of variance (ANOVA) and statistics fitness of thermal conductivity, specific heat capacity, thermal stability, and viscosity.

Source	Thermal conductivity (W/m.K)				
	Sum of Squares	df	Mean Square	F-value	P-value
Model	0.0923	2	0.0462	147.88	< 0.0001
A-[EMM][OSO4]+DG+MXene	0.0368	1	0.0368	117.87	< 0.0001
B-Temperature	0.0555	1	0.0555	177.89	< 0.0001
AB	N/A	N/A	N/A	N/A	N/A
A²	N/A	N/A	N/A	N/A	N/A
B²	N/A	N/A	N/A	N/A	N/A
Residual	0.0031	10	0.0003		
Lack of Fit	0.0027	6	0.0005	4.77	0.0762
Pure Error	0.0004	4	0.0001		
Cor Total	0.0954	12			
R²					0.9673
Adjusted R²					0.9608
Predicted R²					0.9129
Adequate Precision					35.3329
Std. Dev.					0.0177
Mean					0.6429
C.V. %					2.75

Source	Specific Heat Capacity (J/(g.K))				
	Sum of Squares	df	Mean Square	F-value	P-value
Model	0.3300	2	0.1650	43.61	< 0.0001
A-[EMM][OSO4]+DG+MXene	0.1210	1	0.1210	31.98	0.0002
B-Temperature	0.2090	1	0.2090	55.23	< 0.0001
AB	N/A	N/A	N/A	N/A	N/A
A²	N/A	N/A	N/A	N/A	N/A
B²	N/A	N/A	N/A	N/A	N/A
Residual	0.0378	10	0.0038		
Lack of Fit	0.0331	6	0.0055	4.68	0.0785
Pure Error	0.0047	4	0.0012		
Cor Total	0.3679	12			
R²					0.8971
Adjusted R²					0.8766
Predicted R²					0.8204
Adequate Precision					19.1382
Std. Dev.					0.0615
Mean					2.26
C.V. %					2.72

Source	Thermal Stability (wt. loss %)				
	Sum of Squares	df	Mean Square	F-value	P-value
Model	0.2217	2	0.1109	60.33	< 0.0001
A-[EMM][OSO4]+DG+MXene	0.0019	1	0.0019	1.05	0.3291
B-Temperature	0.2198	1	0.2198	119.61	< 0.0001
AB	N/A	N/A	N/A	N/A	N/A
A²	N/A	N/A	N/A	N/A	N/A
B²	N/A	N/A	N/A	N/A	N/A
Residual	0.0184	10	0.0018		
Lack of Fit	0.0165	6	0.0028	5.90	0.0538
Pure Error	0.0019	4	0.0005		
Cor Total	0.2401	12			
R²					0.9235
Adjusted R²					0.9082
Predicted R²					0.8217
Adequate Precision					22.0863
Std. Dev.					0.0429
Mean					0.5996
C.V. %					7.15

Source	Viscosity (mPa.s)				
	Sum of Squares	df	Mean Square	F-value	P-value
Model	660.24	5	132.05	118.08	< 0.0001
A-[EMM][OSO4]+DG+MXene	141.12	1	141.12	126.20	< 0.0001
B-Temperature	475.73	1	475.73	425.42	< 0.0001
AB	0.0226	1	0.0226	0.0202	0.8910
A²	19.76	1	19.76	17.67	0.0040
B²	31.81	1	31.81	28.44	0.0011
Residual	7.83	7	1.12		
Lack of Fit	3.14	3	1.05	0.8953	0.5169
Pure Error	4.68	4	1.17		
Cor Total	668.07	12			
R²					0.9883
Adjusted R²					0.9799
Predicted R²					0.9526
Adequate Precision					35.3415
Std. Dev.					1.06
Mean					19.40
C.V. %					5.45

3.3.1 Parametric analysis of thermal conductivity

Figure 15 presents the combined effect of temperature and nanoparticles concentration on thermal conductivity. Model fitness was confirmed statically. The model F-value of 147.88 implies the model is significant, as shown from the analysis of variance (ANOVA) in Table 4. There is only a 0.01% chance that this large F-value could occur due to noise. P-values less than 0.0500 indicate model terms are significant. In this case, A and B are efficient model terms. The Lack of Fit F-value of 4.77 implies a 7.62% chance that a large lack of Fit F-value could occur due to noise. Non-significant Lack of fit is satisfactory to model fitness.

The results show that an increase in temperature and nanoparticles concentration improved the thermal conductivity, as shown in the 3D response surface and 2D contour graph in Figure 15. With the increase in temperature, the kinetic energy of the molecules moves faster, which increases the thermal conductivity of the studied fluid. R^2, Adjusted R^2 and Predicted R^2 of thermal conductivity were above 0.90, showing reasonable agreement that data is quite fit model will predict closest to real response value. Adequate precision measures the signal-to-noise ratio. A ratio greater than 4 is desirable. The current model ratio is 35.333 indicates an adequate signal. This model can be used to navigate the design space. Figure 16a presented the actual experimental value vs. model predicted value; values are close to the ideal line. The perturbation plot in Figure 16b shows the positive effect of temperature and nanoparticles concentration on the thermal conductivity. However, among both inputs, the temperature has a more positive impact on response as compared to nanoparticles concentration as it observed that line B (temperature) in the perturbation plot has a steep slope. The linear equation (Eq 6) in terms of actual factors can be used to predict the response for given levels of each factor. Here, the levels should be specified in the original units for each factor.

$$\text{Thermal conductivity} = -1.39061 + 0.642069A + 0.005715B \tag{6}$$

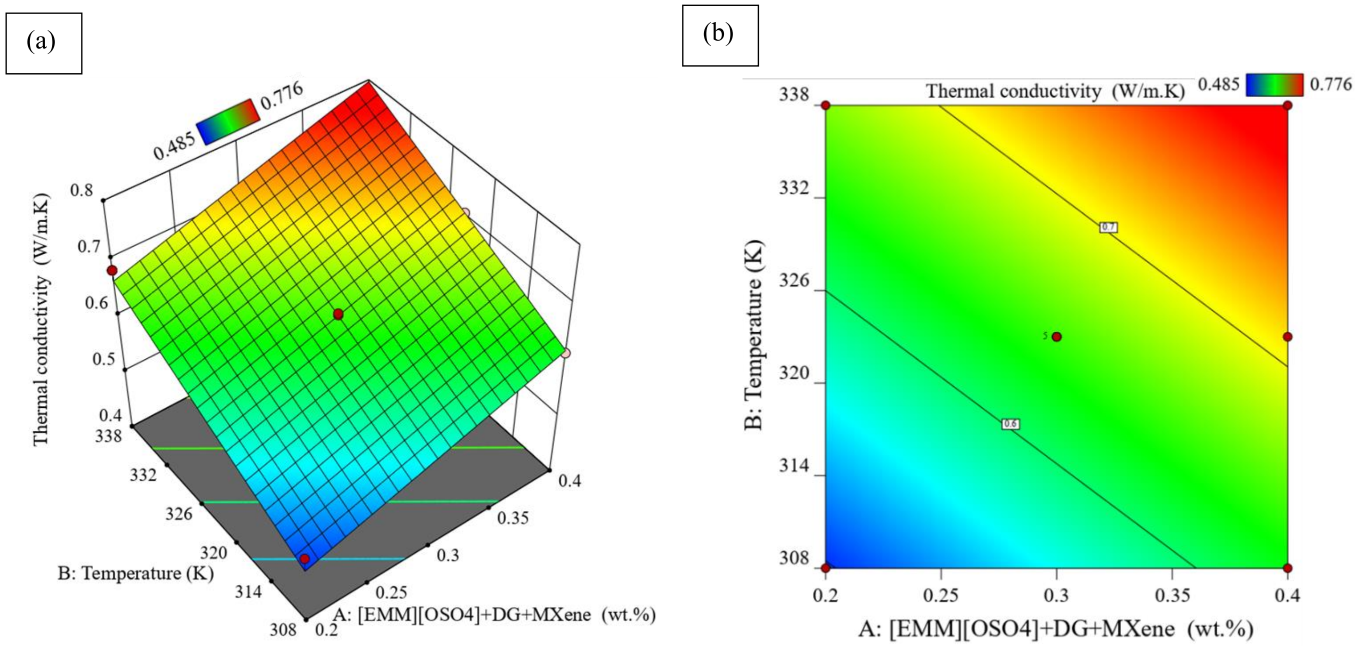

Figure 15: (a) 3D response (b) 2D contour graph of thermal conductivity at combined effect of temperature (K) and [EMM][OSO_4]+DG+MXene (wt.%).

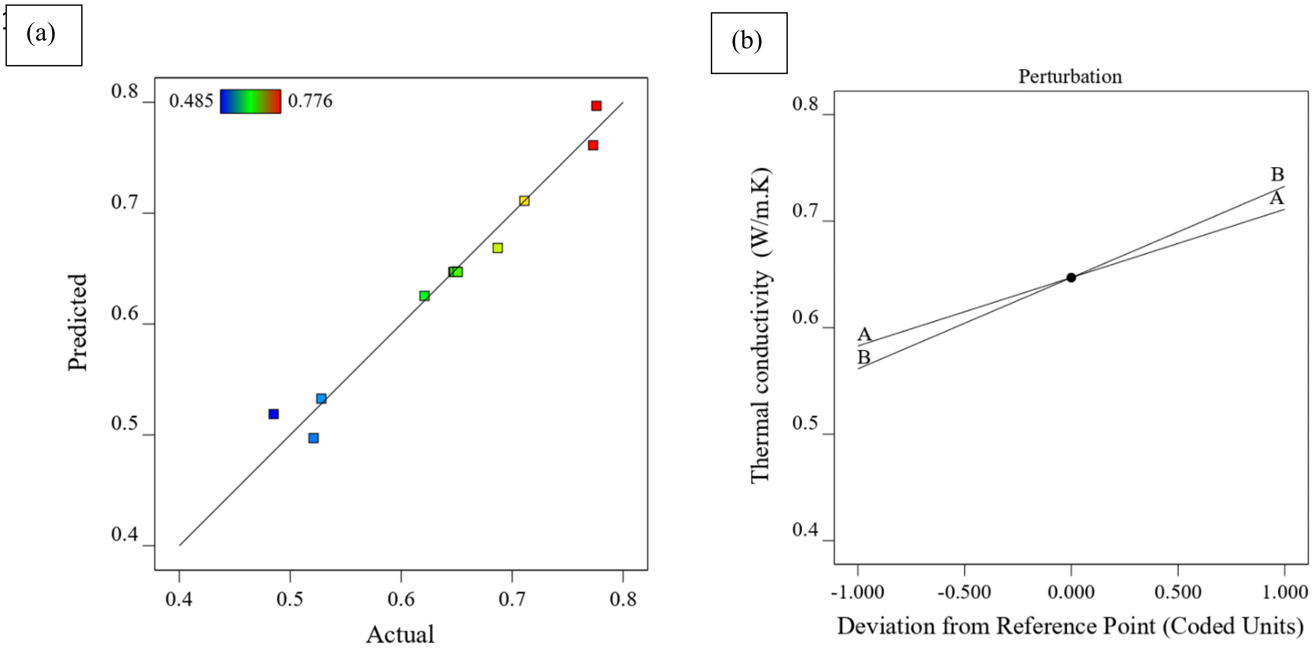

Figure 16: (a) Actual vs. predicted (b) Perturbation plot of thermal conductivity at A: temperature (K) and B: [EMM][OSO_4]+DG+MXene (wt.%).

3.3.2 Parametric analysis of specific heat capacity

The combined effect of temperature and nanoparticles concentration on specific heat capacity is depicted in Figure 17. A high model Model F-value of 43.61 and low P-values less than 0.0500 indicate model fitness. Both model terms, nanoparticles concentration (A) and temperature (B), are significant. Lack of Fit was found non-significant due to low F-value and high P-value of 0.0785 that greater than 0.05 as presented in ANOVA in Table 4. A specific heat capacity shows that an increase in temperature increases the specific heat capacity. Due to the temperature rise, the molecules of the fluids start to vibrate and jump to a higher energy state resulting in increased specific heat capacity. However, nanoparticles concentration causes a decreased specific heat capacity, as shown in the 3D response (Figure 17a) and 2D contour graph (Figure 17b). The high concentration of nanoparticles in the studied fluid makes the molecules difficult to jump from a lower energy state to a higher energy state resulting in decreased specific heat capacity) Figure 18a shows the actual experimental value vs. model predicted value. The fitness statistics show that R^2 of 0.8971, adjusted R^2 of 0.8766, and Predicted R^2 of 0.8204. Predicted R^2 has a reasonable agreement with the Adjusted R^2 as the difference is less than 0.2. The perturbation plot in Figure 18b shows that the nanoparticles concentration (A) has a negative effect on specific heat capacity response while temperature (B) has shown a positive effect on specific heat capacity. The mathematical linear correlation equation (Eq. 7) presented the relationship between inputs to response at any given value within the input range.

$$\text{Specific Heat Capacity}=-0.980293-1.16466A+0.011088B \tag{7}$$

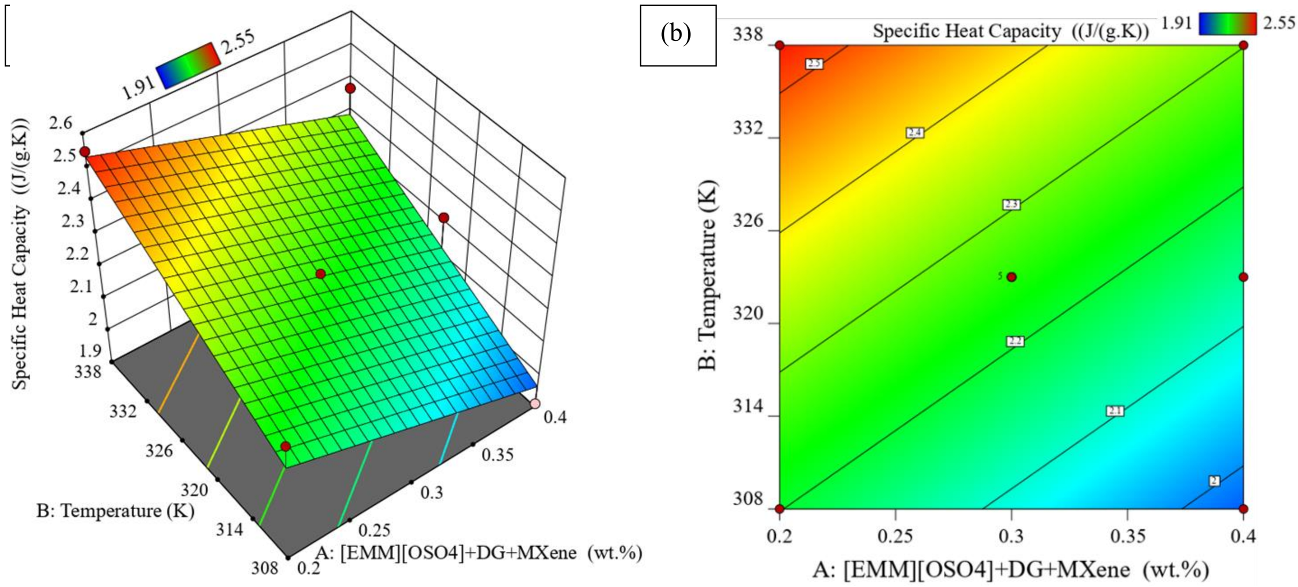

Figure 17: (a) 3D response (b) 2D contour graph of specific heat capacity at the combined effect of temperature (K) and [EMM][OSO_4]+DG+MXene (wt.%).

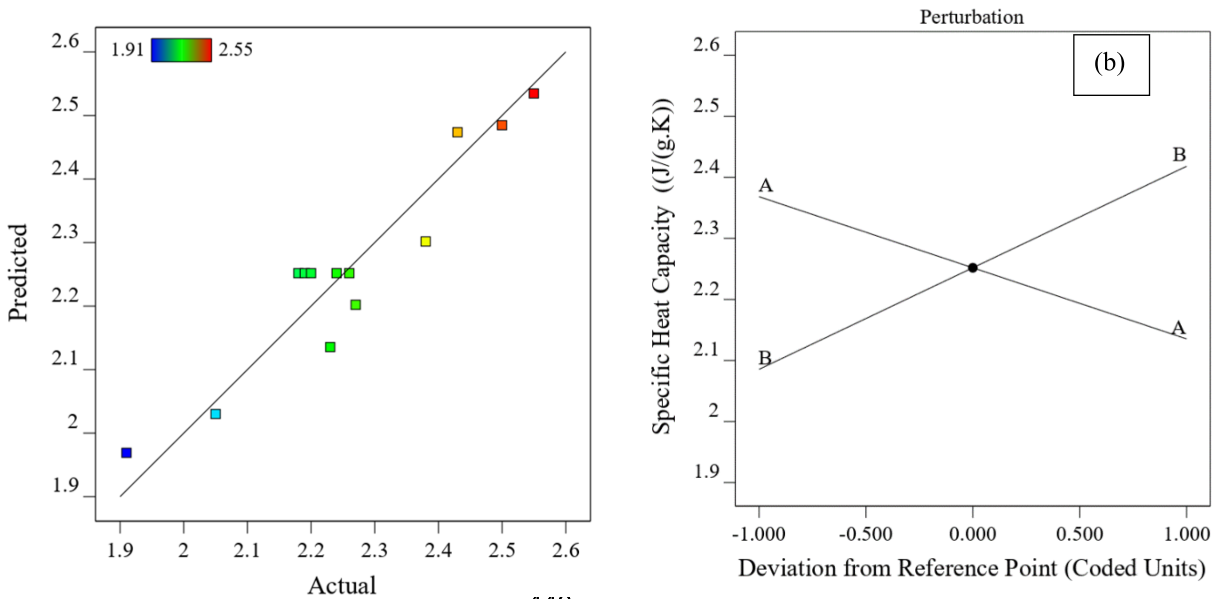

Figure 18: (a) Actual vs predicted (b) Perturbation plot of specific heat capacity at A: temperature (K) and B: [EMM][OSO_4]+DG+MXene (wt.%).

3.3.3 Parametric analysis of thermal stability

The combined effect of temperature and nanoparticles concentration on thermal stability is presented in Figure 19. The thermal stability of nanoparticles decreased with the increase in temperature, as shown from the 3D response and 2D contour graph in Figure 19a and Figure 19b. Nanoparticles evaporate when subjected to heat (high temperature), which decreases their stability in Ionanofluids/nanofluids. However, the concentration of nanoparticles has a marginal effect on thermal stability. A linear model represents the relationship between the response of thermal stability and variable temperature and nanoparticles concentration. The model was fitted well with its F-value of 60.33 and P-value lower than 0.05. In the thermal stability case, B temperature was found significant—however, the concentration of nanoparticles A not significant. Lack of Fit found non-significant, which is good for model fitness. The Adjusted R^2 of 0.9082 is reasonably close to the Predicted R^2 of 0.8217, i.e., the difference is less than 0.2, as shown in Table 4. The actual vs. predicted value graph shows reasonable agreement among it as shown in Figure 20a Perturbation plot of thermal stability at the combined effect of temperature and nanoparticle show negative slow of B temperature and A nanoparticles concentration in Figure 20b. The signal-to-noise ratio is measured by Adequate Precision. It is preferable to have a ratio of more than four. The signal-to-noise ratio of 22.086 for this study suggests a good signal. This model can be used to find your way through the design space. The linear equation (Eq.8) presented the model as;

$$\text{Thermal Stability} = +4.31524 - 0.147236A - 0.011370B \tag{8}$$

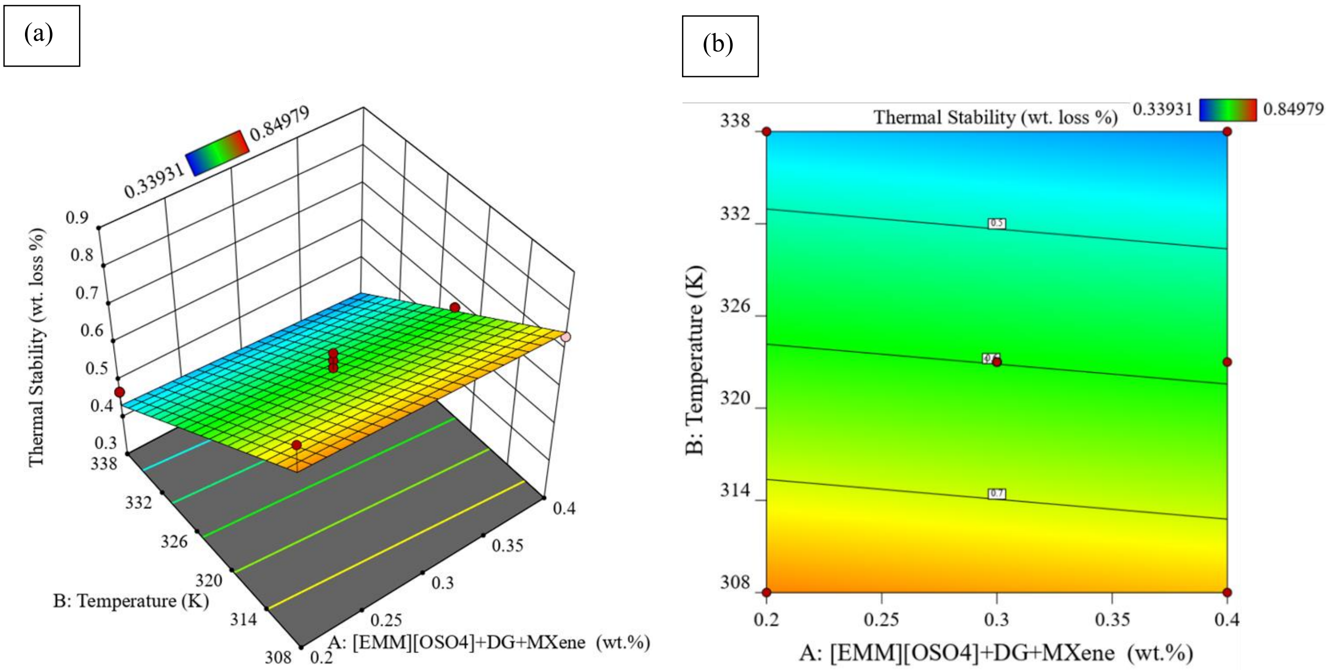

Figure 19: (a) 3D response (b) 2D contour graph of thermal stability at combined effect of temperature (K) and [EMM][OSO_4]+DG+MXene (wt.%).

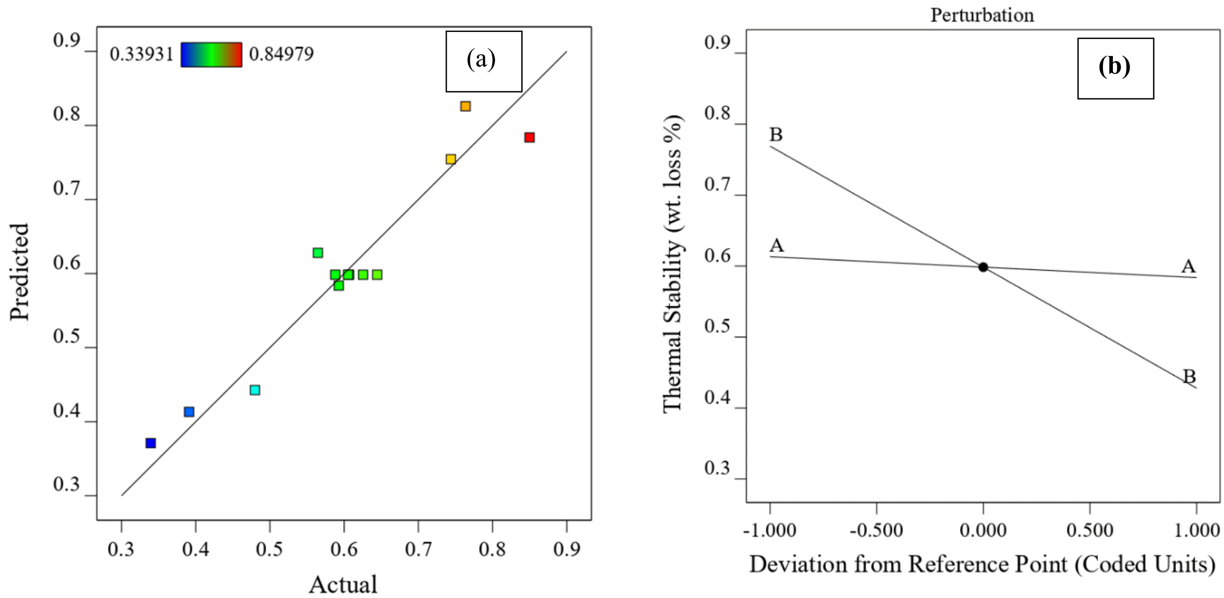

Figure 20: (a) Actual vs. predicted (b) Perturbation plot of thermal stability at A: temperature (K) and B: [EMM][OSO_4]+DG+MXene (wt.%)

3.3.4 Parametric analysis of viscosity

The combined effect of nanoparticles concentration (A) and temperature (B) on viscosity are shown in Figure 21. Polynomial represented the relationship of response viscosity with nanoparticles concentration (A) and temperature (B) parameters. The response of viscosity increases as nanoparticles concentration increases. However, viscosity found decreases as temperature increases, as shown in Figure 21. The molecules of the fluids get separated or distanced further when the temperature is increased, attributed to less cohesive force resulting in decreased viscosity)). The Model F-value of 118.08 indicates that the model is statistically significant. P-values less than 0.0500 imply that model terms are important. In this case, A, B, A^2, B^2 are significant model terms. The Lack of Fit F-value of 0.90 indicates the Lack of Fit is non-significant relative to the pure error. Non-significant lack of fit is good and desirable for the model to fit. The adjusted R^2 of 0.9799 is reasonably close to the predicted R^2 of 0.9526; i.e., the difference is less than 0.2, as shown in Table 4. The actual vs. predicted value presented a good agreement, as presented in Figure 22a. The perturbation plot of viscosity shows that both parameters influence the response. However, the temperature is negative, and nanoparticles positively affect viscosity response, as shown in Figure 22b. As given below, a polynomial quadratic equation (9) represented the relationship between response viscosity and nanoparticle concentration and temperature.

$$\text{Viscosity}=+1265.04836-19.73823A-7.22201B-0.050100AB+139.19889A^2+0.010384B^2 \quad (9)$$

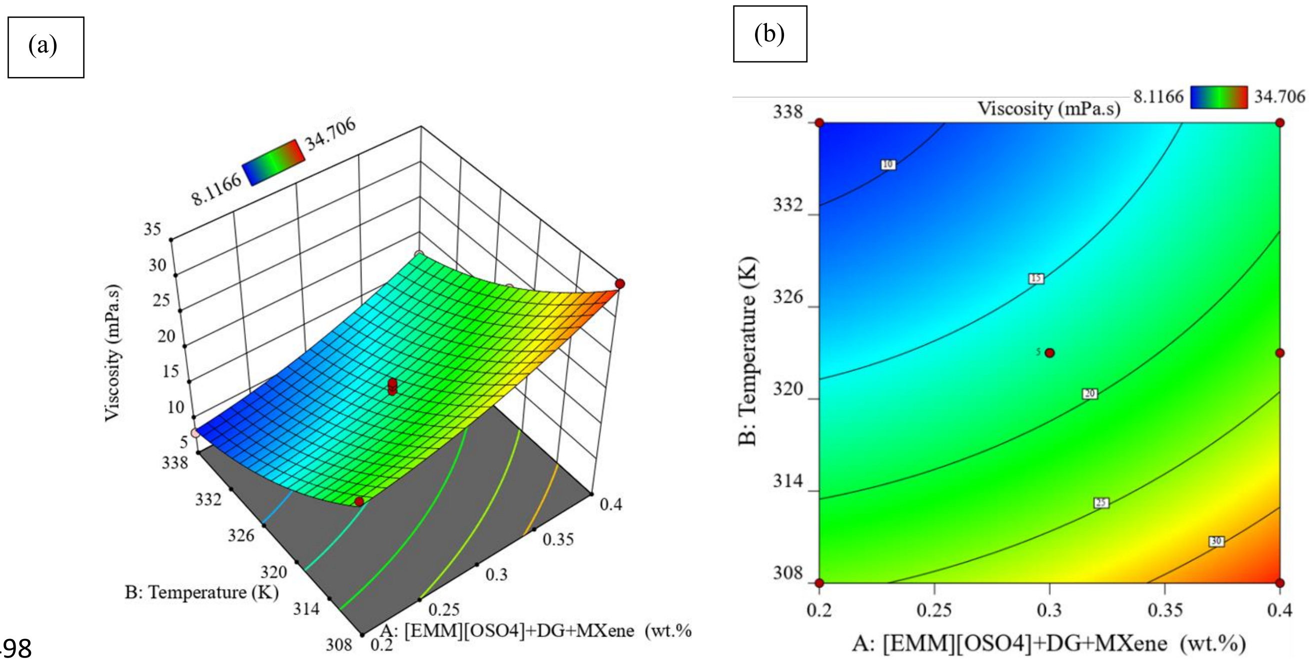

Figure 21: (a) 3D response (b) 2D contour graph of viscosity at combined effect of temperature (K) and [EMM][OSO_4]+DG+MXene (wt.%).

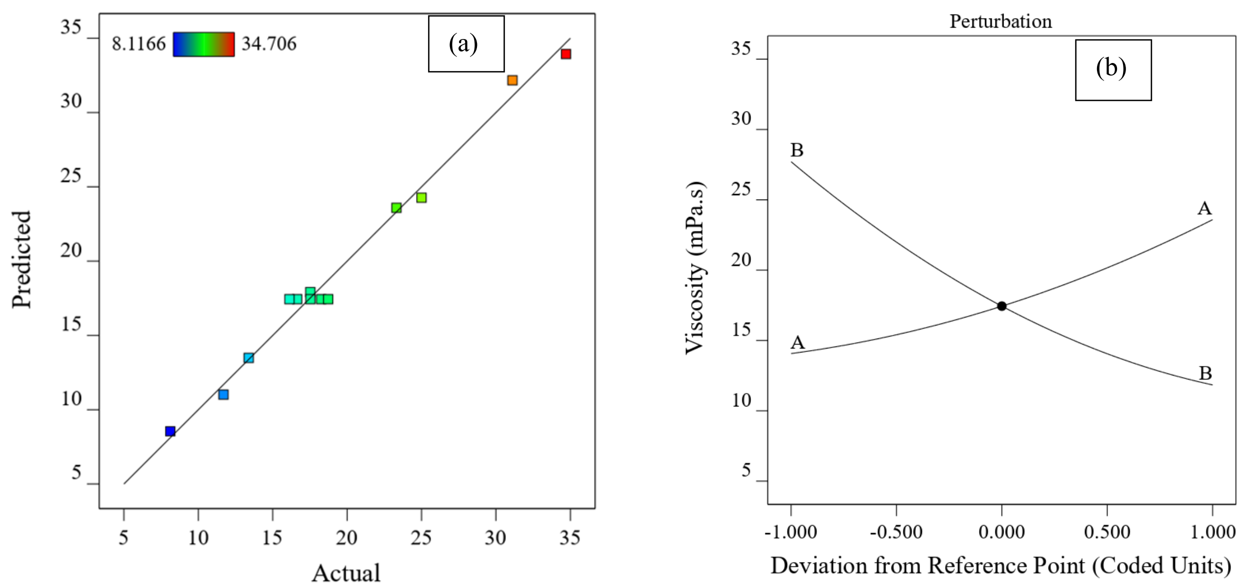

Figure 22: (a) Actual vs predicted (b) Perturbation plot of viscosity at A: temperature (K) and B: [EMM][OSO_4]+DG+MXene (wt.%).

Optimized thermophysical properties of thermal conductivity (0.776 W/m.K), specific heat capacity (2.5 J/g.K), thermal stability (0.33931 wt. loss %), and viscosity (11.696 mPa.s) of MXene Ionanofluids were obtained at a temperature of 343 K and nanofluids concentration of 0.3 wt.%. These optimized thermophysical properties of MXene Ionanofluids could improve the performance of hybrid solar photovoltaic and thermal systems when MXene Ionanofluids will use as heat transfer medium.

4 Conclusions

This section concludes with a discussion of the observations based on the results obtained. The study's findings are utilized to determine if the stated hypotheses are supported, and the study's research objectives are eventually evaluated. The observations are discussed based on the performance of the LMBPN models and the parametric analysis of the RSM models. Finally, the study's contributions are explored by utilizing methodological and analytical perspectives.

- A new predictive network framework for thermophysical properties of Mxene Ionanofluids is developed using an LMBP training algorithm based on multilayer neural networks.
- In the first instance, the architecture of the proposed ANN model is shown. The standardized LMBP algorithms were then learned to produce effective models for respective thermophysical properties.
- It has been discovered that the hidden neurons in the hidden layer play a crucial role in precise prediction. The developed algorithms can accurately predict thermophysical properties in training testing and validation stages.
- The results indicate that the built LMBP network estimates the thermophysical properties accurately, and the performance demonstrates the viability and efficiency of the algorithm concerning the accuracy of the estimation.
- RSM model was well fitted to thermophysical properties of MXene Ionanofluids. A correlation was developed among inputs paraments of [EMM][OSO_4]+DG+MXene concentration (wt.%) and temperature (K) with outputs thermophysical properties of MXene Ionanofluids.
- Application of MXene Ionanofluids at optimized thermophysical properties could potentially improve the performance of hybrid solar photovoltaic and thermal systems.
- The suggested framework has dynamic functional importance and can be used in the future to assist engineers or researchers in evaluating the thermal properties' behavior.

- Furthermore, the obtained results can be used by the academic and industrial communities to determine the best conditions for synthesizing high efficient MXene ionanofluids within minimum time in order to enhance the efficiency of PV/T systems.
- The developed ANN model can not only predict MXene Ionanofluids' behaviour, but it can also reduce lab expenditures by eliminating the extraction of experimental findings.
- Additionally, experimentation with other parameters or the same parameters used in this work with different boundaries are highly advised for an enhanced heat transfer fluid.
- Finally, the suggested Levenberg Marquardt optimized ANN, and RSM based optimization might serve as useful references for future research of MXene based heat transfer fluids in PVT systems.

Acknowledgment: Throughout the study, the authors are grateful to the Ratchadapisek Somphot Fund for Artificial Intelligence, Machine Learning, and Smart Grid Technology Research Unit, as well as the Chulalongkorn University Postdoctoral Fellowship and the Second Century Fund (C2F).

References

[1] L. Das *et al.*, "Hydrothermal performance improvement of an inserted double pipe heat exchanger with Ionanofluid," *Case Studies in Thermal Engineering,* vol. 28, p. 101533, 2021.

[2] M. Faizan, R. Ahmed, and H. M. Ali, "A critical review on thermophysical and electrochemical properties of Ionanofluids (nanoparticles dispersed in ionic liquids) and their applications," *Journal of the Taiwan Institute of Chemical Engineers,* 2021.

[3] J. M. Alizadeh, Mostafa Keshavarz "An experimental evaluation on thermophysical properties of functionalized graphene nanoplatelets ionanofluids," *International Communications in Heat and Mass Transfer,* vol. 98, pp. 31-40, 2018.

[4] A. Agresti *et al.*, "Titanium-carbide MXenes for work function and interface engineering in perovskite solar cells," *Nature materials,* vol. 18, no. 11, pp. 1228-1234, 2019.

[5] B. Bakthavatchalam *et al.*, "Optimization of thermophysical and rheological properties of mxene ionanofluids for hybrid solar photovoltaic/thermal systems," *Nanomaterials,* vol. 11, no. 2, p. 320, 2021.

[6] A. Abdelrazik, K. Tan, N. Aslfattahi, A. Arifutzzaman, R. Saidur, and F. Al-Sulaiman, "Optical, stability and energy performance of water-based MXene nanofluids in hybrid PV/thermal solar systems," *Solar Energy,* vol. 204, pp. 32-47, 2020.

[7] N. Aslfattahi *et al.*, "Efficiency enhancement of a solar dish collector operating with a novel soybean oil-based-MXene nanofluid and different cavity receivers," *Journal of Cleaner Production,* vol. 317, p. 128430, 2021.

[8] L. A. Samylingam, Navid Saidur, R Yahya, Syed Mohd Afzal, Asif Arifutzzaman, A Tan, KH Kadirgama, K "Thermal and energy performance improvement of hybrid PV/T system by using

olein palm oil with MXene as a new class of heat transfer fluid," *Solar Energy Materials and Solar Cells,* vol. 218, p. 110754, 2020.

[9] F. Bayrak, H. F. Oztop, and A. Hepbasli, "Energy and exergy analyses of porous baffles inserted solar air heaters for building applications," *Energy Buildings,* vol. 57, pp. 338-345, 2013.

[10] J. R. D. Rabunal, Julian, *Artificial neural networks in real-life applications*. United States of America: IGI Global, 2006.

[11] J. Z. Wang, Yuling Yao, Peitao Ma, Mingyan Wang, Hua "Established prediction models of thermal conductivity of hybrid nanofluids based on artificial neural network (ANN) models in waste heat system," *International Communications in Heat and Mass Transfer,* vol. 110, p. 104444, 2020.

[12] F. Ö. Selimefendigil, Hakan F, "Numerical study and pod-based prediction of natural convection in a ferrofluids–filled triangular cavity with generalized neural networks," *Numerical Heat Transfer, Part A: Applications,* vol. 67, no. 10, pp. 1136-1161, 2015.

[13] X. B. Yang, Ahmadreza Wen, Shiwei Toghraie, Davood Soltani, Farid "Applying Artificial Neural Networks (ANNs) for prediction of the thermal characteristics of water/ethylene glycol-based mono, binary and ternary nanofluids containing MWCNTs, titania, and zinc oxide," *Powder Technology,* vol. 388, pp. 418-424, 2021.

[14] W. Y. Ji, Liu Chen, Zihan Mao, Mao Huang, Jia-nan "Experimental studies and ANN predictions on the thermal properties of TiO2-Ag hybrid nanofluids: Consideration of temperature, particle loading, ultrasonication and storage time," *Powder Technology,* vol. 388, pp. 212-232, 2021.

[15] S. A. Tian, Noreen Izza Toghraie, Davood Eftekhari, S Ali and M. Hekmatifar, "Using perceptron feed-forward Artificial Neural Network (ANN) for predicting the thermal conductivity of graphene oxide-Al2O3/water-ethylene glycol hybrid nanofluid," *Case Studies in Thermal Engineering,* vol. 26, p. 101055, 2021.

[16] M. S. Malika, Shriram S "Application of RSM and ANN for the prediction and optimization of thermal conductivity ratio of water based Fe2O3 coated SiC hybrid nanofluid," *International Communications in Heat and Mass Transfer,* vol. 126, p. 105354, 2021.

[17] A. Abidi, A. I. Khdair, and R. Kalbasi, "Using ANN techniques to forecast thermal performance of a vacuum tube solar collector filled with SiO2/EG-water nanofluid," *Journal of the Taiwan Institute of Chemical Engineers,* vol. 128, pp. 301-313, 2021.

[18] B. Bakthavatchalam, N. B. Shaik, and P. B. Hussain, "An artificial intelligence approach to predict the thermophysical properties of MWCNT nanofluids," *Processes,* vol. 8, no. 6, p. 693, 2020.

[19] A. S. Geetha, J Sundaram, K Mohana Usha, S Thentral, TM Thamizh Boopathi, CS Ramya, R Sathyamurthy, Ravishankar "Prediction of hourly solar radiation in Tamil Nadu using ANN model with different learning algorithms," *Energy Reports,* vol. 8, pp. 664-671, 2022.

[20] F. Selimefendigil, H. F. Öztop, and M. Afrand, "Shape effects of TEG mounted ventilated cavities with alumina-water nanofluids on the performance features by using artificial neural networks," *Engineering Analysis with Boundary Elements,* vol. 140, pp. 79-97, 2022.

[21] F. Selimefendigil and H. F. Öztop, "Thermoelectric generation in bifurcating channels and efficient modeling by using hybrid CFD and artificial neural networks," *Renewable Energy,* vol. 172, pp. 582-598, 2021.

[22] N. Parashar, N. Aslfattahi, S. M. Yahya, and R. Saidur, "ANN modeling of thermal conductivity and viscosity of MXene-based aqueous ionanofluid," *International Journal of Thermophysics,* vol. 42, no. 2, pp. 1-24, 2021.

[23] N. Parashar, N. Aslfattahi, S. M. Yahya, and R. Saidur, "An artificial neural network approach for the prediction of dynamic viscosity of MXene-palm oil nanofluid using experimental data," *Journal of Thermal Analysis and Calorimetry,* vol. 144, no. 4, pp. 1175-1186, 2021.

[24] C. Boobalan and S. K. Kannaiyan, "A correlation to predict the thermal conductivity of MXene-silicone oil based nano-fluids and data driven modeling using artificial neural networks," *International Journal of Energy Research,* 2022.

[25] N. B. Shaik, S. R. Pedapati, S. A. A. Taqvi, A. Othman, and F. A. A. Dzubir, "A Feed-Forward Back Propagation Neural Network Approach to Predict the Life Condition of Crude Oil Pipeline," *Processes,* vol. 8, no. 6, p. 661, 2020.

[26] N. B. Shaik, S. R. Pedapati, and F. A. B. Dzubir, "Remaining useful life prediction of a piping system using artificial neural networks: A case study," *Ain Shams Engineering Journal,* 2021.

[27] N. B. Shaik *et al.*, "Corrosion behavior of LENS deposited CoCrMo alloy using Bayesian regularization-based artificial neural network (BRANN)," *Journal of Bio-and Tribo-Corrosion,* vol. 7, no. 3, pp. 1-13, 2021.

[28] N. B. Shaik, S. R. Pedapati, A. Othman, K. Bingi, and F. A. Abd Dzubir, "An intelligent model to predict the life condition of crude oil pipelines using artificial neural networks," *Neural Computing and Applications,* pp. 1-22, 2021.

[29] M. Inayat, S. A. Sulaiman, A. Inayat, N. B. Shaik, A. R. Gilal, and M. Shahbaz, "Modeling and parametric optimization of air catalytic co-gasification of wood-oil palm fronds blend for clean syngas (H2+CO) production," *International Journal of Hydrogen Energy,* vol. 46, no. 59, pp. 30559-30580, 2021/08/26/ 2021, doi: https://doi.org/10.1016/j.ijhydene.2020.10.268.

[30] M. Inayat, S. A. Sulaiman, and J. C. Kurnia, "Catalytic co-gasification of coconut shells and oil palm fronds blends in the presence of cement, dolomite, and limestone: Parametric optimization via Box Behnken Design," *Journal of the Energy Institute,* vol. 92, no. 4, pp. 871-882, 2019/08/01/ 2019, doi: https://doi.org/10.1016/j.joei.2018.08.002.

[31] S. Karimipour, R. Gerspacher, R. Gupta, and R. J. Spiteri, "Study of factors affecting syngas quality and their interactions in fluidized bed gasification of lignite coal," *Fuel,* vol. 103, pp. 308-320, 2013/01/01/ 2013, doi: https://doi.org/10.1016/j.fuel.2012.06.052.

[32] A. Arami-Niya, W. M. A. Wan Daud, F. S. Mjalli, F. Abnisa, and M. S. Shafeeyan, "Production of microporous palm shell based activated carbon for methane adsorption: Modeling and optimization using response surface methodology," *Chemical Engineering Research and Design,* vol. 90, no. 6, pp. 776-784, 2012/06/01/ 2012, doi: https://doi.org/10.1016/j.cherd.2011.10.001.

[33] S. Yusup, Z. Khan, M. M. Ahmad, and N. A. Rashidi, "Optimization of hydrogen production in in-situ catalytic adsorption (ICA) steam gasification based on Response Surface Methodology," *Biomass and Bioenergy,* vol. 60, pp. 98-107, 1// 2014, doi: http://dx.doi.org/10.1016/j.biombioe.2013.11.007.